

# Observation of the Chern-Simons gauge anomaly

Sunil Mittal<sup>1,2</sup>, Sriram Ganeshan<sup>1,3</sup>, Jingyun Fan<sup>1</sup>, Abolhassan Vaezi<sup>4</sup>,  
Mohammad Hafezi<sup>1,2,†</sup>

<sup>1</sup>Joint Quantum Institute, NIST/University of Maryland, College Park MD 20742, USA

<sup>2</sup>Department of Electrical Engineering and Institute for Research in Electronics and Applied Physics, University of Maryland, College Park MD 20742, USA

<sup>3</sup>Condensed Matter Theory Center, University of Maryland, College Park MD 20742, USA

<sup>4</sup>Laboratory of Atomic and Solid State Physics, Cornell University, Ithaca NY 14853, USA

†hafezi@umd.edu

Topological Quantum Field Theories (TQFTs) are powerful tools to describe universal features of topological orders. A hallmark example of a TQFT is the 2+1 D Chern-Simons (CS) theory which describes topological properties of both integer and fractional quantum Hall effects. The gauge invariant form of the CS theory with boundaries, encompassing both edge and bulk terms, provides an unambiguous way to relate bulk topological invariants to the edge dynamics. This bulk-edge correspondence is manifested as a gauge anomaly of the chiral dynamics at the edge, and provides a direct insight into the bulk topological order. Such an anomaly has never been directly observed in an experiment. In this work, we experimentally implement the integer quantum Hall model in a photonic system, described by the corresponding CS theory. By selectively manipulating and probing the edge, we exploit the gauge anomaly of the CS theory, for the first time. The associated spectral edge flow allows us to unambiguously measure topological invariants, i.e., the winding number of the edge states. This experiment provides a new approach for direct measurement of topological invariants, independent of the microscopic details, and thus could be extended to probe strongly correlated topological orders.

TQFTs not only provide an elegant theoretical description of the universal features of topological order, but have also played a vital role in predicting key experimental signatures [1, 2]. With the recent explosion of interest in topological insulators [3–5], TQFTs, such as the CS theory, have become pivotal in understanding various symmetry protected and symmetry broken topological phases [6]. Following the pioneering work of Witten [7] on the CS theory, X-G. Wen [8] and Fröhlich-Kerler [9] showed that the low energy limit of a quantum Hall system can be described by the CS theory, thereby explaining the discreteness of the Hall conductivity.

Recently, there has been a surge of interest in investigating topological states, with synthetic gauge fields, in various atomic [10–13] and photonic systems [14, 15]. In particular, topological robustness of photonic transport was quantitatively confirmed both in the microwave [16] and telecom domains [17], using synthetic 2D structures. Moreover, topological photonic edge states have been imaged in two concurrent experiments [18, 19]. At the same time, one-dimensional photonic systems with topological features have been also investigated [20–22].

Experimental signatures of quantum Hall states in photonic systems have so far relied on the microscopic description of the implemented model [23–25]. Thus, it is desirable to develop experimental tools for photonic systems that can access the topological states from a universal perspective. Universal features of the quantum Hall states can be defined using the CS theory which, unlike the microscopic model, can be extended to the low energy regime of strongly correlated topological phases. One of the remarkable features of the CS theory is the gauge anomaly which connects the bulk topological phase to the anomalous chiral dynamics at the boundary. In this work, we first explain how this anomaly is manifested in a photonic system, and then, we experimentally demonstrate that this anomalous behavior can be exploited to measure topological invariants. For this demonstration, we employ the unique ability of our photonic system to selectively manipulate edge states — a feature that is challenging to achieve in current electronic systems.

The effective CS action that yields the quantized Hall current in the bulk is given by

$$S_{cs}^{\Sigma}[A] = \frac{1}{4\pi k} \int_{\Sigma} d^2x dt \epsilon^{\mu\nu\lambda} A_{\mu} \partial_{\nu} A_{\lambda}. \quad (1)$$

where  $A_{\mu}$  is the bulk gauge field in the region  $\Sigma$ , and  $k$  is an integer index that labels the bulk topological

phase (i.e., the Chern number), and its quantization is encoded in the definition of the CS action [8]. Remarkably, this action captures both non-interacting ( $k = 1$ ) and strongly correlated systems, for example, the 1/2-Laughlin state ( $k = 2$ ) for bosons. For a quantum Hall system with no boundaries, e.g. a sphere, this action is gauge invariant. However, the action is not gauge invariant for a system with boundaries, e.g., a disk. In order to make the system gauge invariant, one has to couple the CS theory to a (1+1)D conformal field theory of chiral bosons at the edge. More precisely, the gauge invariant action describing the quantum Hall system on a manifold  $(\Sigma \times R)$  with boundary  $(R)$  is given by  $S = S_{cs}^{\Sigma \times R}[A_\mu] + S^R[\phi, \eta_\mu]$  where the edge action [26, 27] is

$$S^R[\phi, \eta_\mu] = \frac{1}{4\pi} \int_R dx dt [k D_t \phi D_x \phi - vk (D_x \phi)^2 - \epsilon^{\mu\nu} \eta_\mu \partial_\nu \phi]. \quad (2)$$

The edge action describes the dynamics of bosonic excitations  $\phi$  of the underlying edge degrees of freedom, which may be either bosons or fermions.  $v$  is the velocity of the edge modes. We have defined the covariant derivative as  $D_\mu \phi = \partial_\mu \phi - \frac{1}{k} \eta_\mu$  and  $\eta_\mu = A_\mu|_R$  is the gauge field at the boundary. The overall action is then gauge invariant under the transformation  $A_\mu \rightarrow A_\mu + \partial_\mu \beta$ ,  $\eta_\mu \rightarrow \eta_\mu + \partial_\mu \beta$  and  $\phi \rightarrow \phi - \frac{1}{k} \beta$ . Note that the prefactor  $k$  in  $S^R[\phi, \eta_\mu]$  is the winding number of the edge states, and is chosen to be the same as in Eq.(1) to guarantee the gauge invariance. Evidently,  $S^R[\phi, \eta_\mu]$  by itself is not gauge invariant, and therefore, by coupling a gauge field, in form of an external magnetic field acting only on the edge, one can reveal this gauge anomaly.

This gauge anomaly manifests as a *spectral flow* of the edge states as a function of the flux  $\theta$ , which can be directly observed in an experiment as the flow of transmission resonances. Specifically, if we define a charge operator which carries  $q = m/k$  units of particle number where  $m = 1, \dots, k$ , one can show that the corresponding energy is

$$E_q = v \left( p - q \frac{\theta}{L} \right), \quad (3)$$

where  $p$  is the momentum along the edge of the length  $L$  (see SI). Such spectrum flows as a function of the coupled flux. This spectral flow can be also understood by noting that in the presence of gauge field, for charge excitations, the momentum operator must be replaced by the covariant momentum operator,  $p - q \frac{\theta}{L}$ . For instance, consider the charge with  $q = 1$  for non-interacting photons. Due to the quantization of momentum at the edge as  $p_n = n \frac{2\pi}{L}$ , inserting  $\theta = 2\pi$  flux causes  $p_n \rightarrow p_{n-1}$  for these charge excitations, and therefore,  $E_n = \frac{2\pi v}{L} (n - \frac{\theta}{2\pi})$ , as shown in Fig. 1a. This spectral flow argument can be generalized for  $q = 1/k$ , as shown in the SI. The origin of this gauge anomaly can be traced back to the fact that the current density of the underlying fundamental particles (e.g. photons) is not conserved, and therefore, gauging the edge leads to the anomalous flow (see SI).

To experimentally observe and measure this gauge anomaly, we implement the integer quantum Hall model in a photonic system: a two dimensional square lattice of ring resonators with a uniform synthetic magnetic field in the bulk and a tunable gauge field coupled only to the lattice edge (Fig. 1b-e). For the uniform part of the magnetic field, we use silicon-on-insulator technology, as previously described in Ref.[18]. To couple a tunable gauge field to the edges, we fabricate 110 nm thick metal (Ti) heaters, positioned above the link ring waveguides on the lattice edge (Fig. 1c-e). These heaters are high resistance metal pads, with typical resistance of 117 Ohms, such that a current flowing through them generates heat and modifies the refractive index, and the accumulated phase of light propagating through the waveguide. A typical heater requires  $\approx 76.5$  mW to introduce a  $2\pi$  phase. Instead of employing a single heater which may introduce a significant disorder in the lattice, we distribute the heaters along the edges while maintaining an accumulated flux of  $2\pi$  (see SI).

We make a square annulus with outer edge of 10 sites and inner edge of 4 sites (Fig. 1b-c), designed to have a uniform magnetic flux  $\alpha = \frac{1}{4}$  per plaquette. This system exhibits two bandgap regions [28]. The first

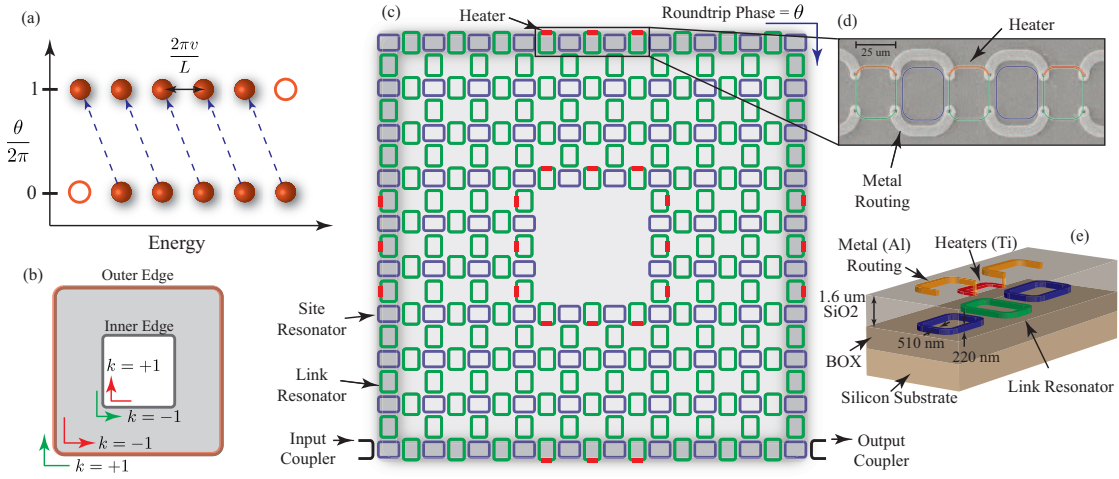


FIG. 1: (a) Spectral flow of edge states with coupled gauge flux  $\theta$  for  $q = 1$  and  $k = 1$ . When  $\theta = 2\pi$ , edge states move by  $k = 1$  positions. (b,c) Square annulus of coupled ring resonators which implements the integer quantum Hall effect. The uniform synthetic magnetic field for photons is introduced by asymmetrically positioning the link rings. The system exhibits two pairs of clockwise and counter clockwise propagating edge states, one each on the outer and the inner edges. The tunable gauge field coupled only to the edge states is introduced by fabricating heaters on link resonators situated on the lattice edges. The total flux  $\theta$  introduced by heaters is the sum of individual phases incurred in link resonator arms. (d) SEM image showing heaters fabricated on top of link resonators (green). (e) Schematic of the waveguide cross section showing the ring resonators, the metal heaters and the metal routing layer.

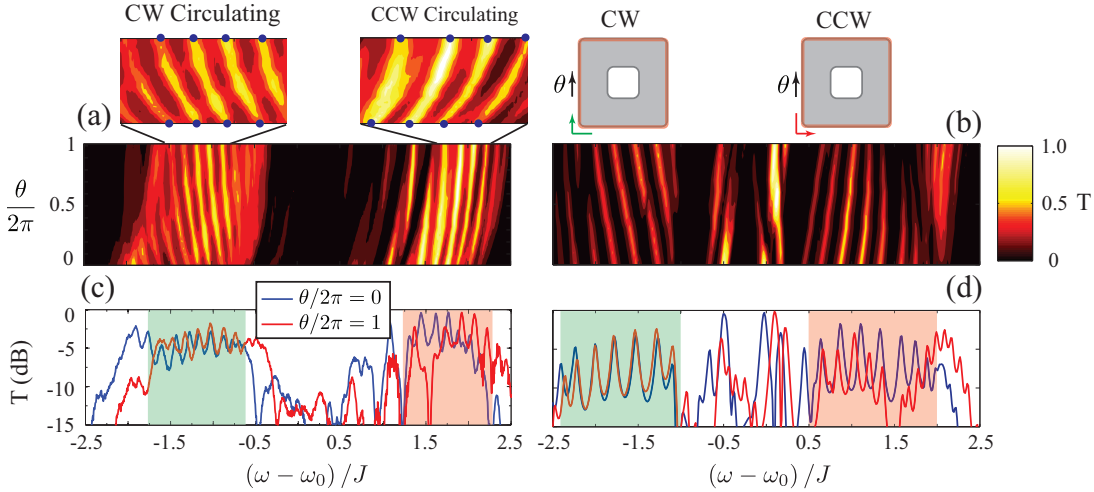


FIG. 2: (a) Measured and (b) simulated transmission (in linear scale, normalized to unity) as a function of phase  $\theta$  and frequency  $\omega$ . For a  $2\pi$  increase in gauge flux, the edge state resonances move by one position, giving  $k = +1.0(1)$  for CW edge band and  $k = -1.0(2)$  for the CCW band. Insets: Zoom-in of the edge state bands. (c) Measured and (d) simulated transmission spectra (in log scale) for  $\theta/2\pi = 0, 1$ . For this  $2\pi$  increase in flux, the measured spectra match approximately in the edge state regions.

(low energy) bandgap corresponds to clockwise (CW) circulating edge states confined on the outer edge, and counter-clockwise (CCW) circulating edge states on the inner edge, as shown with green arrows in Fig. 1b with their corresponding topological invariants (i.e., the winding number). Similarly, the second bandgap (high energy) corresponds to edge states on the outer and the inner edges, but they circulate opposite to those in the first bandgap, as shown in Fig. 1b by red arrows. Fig. 2a,b show the measured and simulated transmission spectra as a function of the coupled flux  $\theta$ . Edge states of the outer edge (bright regions) and the bulk states (dark region in the middle) are easily identifiable. As the coupled flux  $\theta$  increases, the energy of the CW edge states decreases, whereas the energy of CCW edge states increases. For a  $2\pi$  increase in

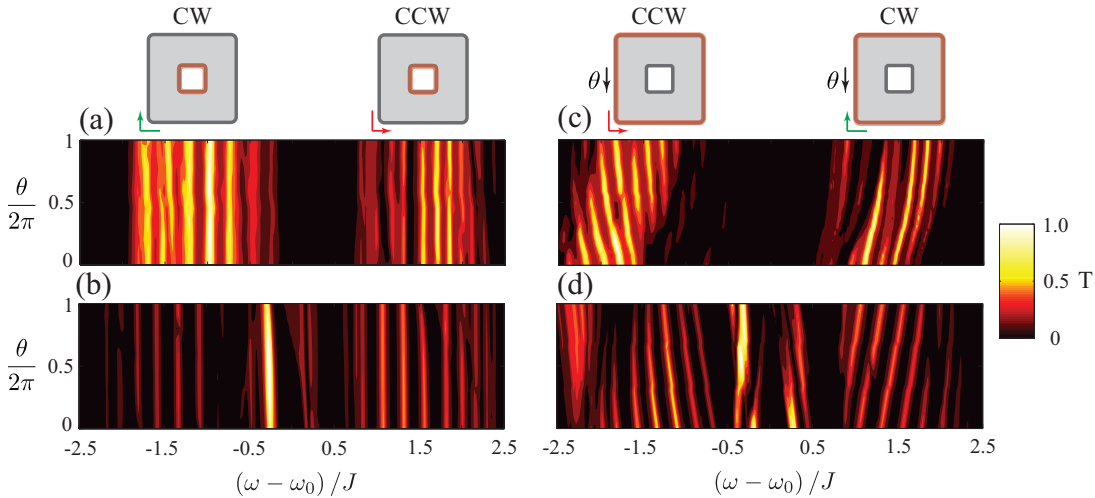


FIG. 3: (a) Measured and (b) simulated transmission spectrum as a function of flux  $\theta$  when only the inner edge is heated. The energies of the edge states associated with the outer edge do not change. (c) Measured and (d) simulated transmission spectrum with spin flipped excitation. The CW and CCW circulating states have now exchanged positions and move in opposite directions (compared to Fig. 2 a,b), giving  $k = -1.2(2)$  for CCW edge band and  $k = +1.2(2)$  for the CW band indicating a sign reversal of integer  $k$ .

flux, the edge state resonances move by one resonance to replace the position once held by its neighbor. Following the above gauge anomaly discussion, this flow indicates that the measured winding number is  $k = +1.0(1)$  for the CW circulating edge states, and  $k = -1.0(2)$  for the CCW circulating edge states. We note that only the outer edge contributes to the transmission spectra, due to the sharpness of the edge states. More specifically, the coupling between the probe waveguides to the inner edge states is exponentially suppressed as  $e^{-d/l_0}$ , where  $d$  is the number of rings between the outer and the inner edge (in this case 4) and  $l_0 = 1/\sqrt{2\pi\alpha} \approx 0.8$  is the magnetic length in units of the lattice spacing. Moreover, such sharpness of edge states allows us to locally create the extra gauge flux  $\theta$  by placing the heaters only on the outmost rings at the boundary.

Fig. 2c,d show the overlap of the observed and simulated transmission spectra at  $\frac{\theta}{2\pi} = 0$  and 1, showing excellent qualitative agreement with the simulation results. We attribute the small discrepancy in the overlap to lattice disorder introduced by the nonlocal response of the heaters. In our design, the heaters are placed 600 nm above the link resonator waveguides. Therefore, in addition to modifying the link resonators, the heaters also modify the resonance frequency of the neighboring sites which adds to the disorder in the lattice (see SI). The discrepancy is more pronounced for the CCW state because of finite size effects in travelling a shorter path from input to the output port.

In order to verify the local character of the gauge coupling, we selectively couple a nonzero flux  $\theta$  to the inner edge by heating the link rings on the inner edge. We observe that heating only the inner edge does not shift the edge states (Fig. 3a,b), which indicates the strong confinement of edge states at the lattice boundary. Furthermore, since our system is time-reversal invariant, it supports two pseudo-spin components, up and down, which circulate in opposite directions in ring resonators [18]. We can selectively excite either pseudo-spin component by appropriately choosing the input port (Fig. 1c). Fig. 3c,d show the measured and simulated transmission spectra as a function of coupled flux  $\theta$ , for a device with spin flipped excitation, compared to Fig.2. At the same time, since the sign of the coupled flux  $\theta$  has also changed, the resulting spectrum becomes similar to Fig.2.

As a control experiment, to investigate the difference of gauge coupling to chiral (anomalous) and non-chiral (non-anomalous) states, we fabricate a ring of resonators (Fig. 4a) which corresponds to a 1D tight-binding model. This system supports topologically trivial Bloch modes, circulating in CW and CCW directions, which are degenerate in the absence of a magnetic flux. Similarly, we couple the flux to these states

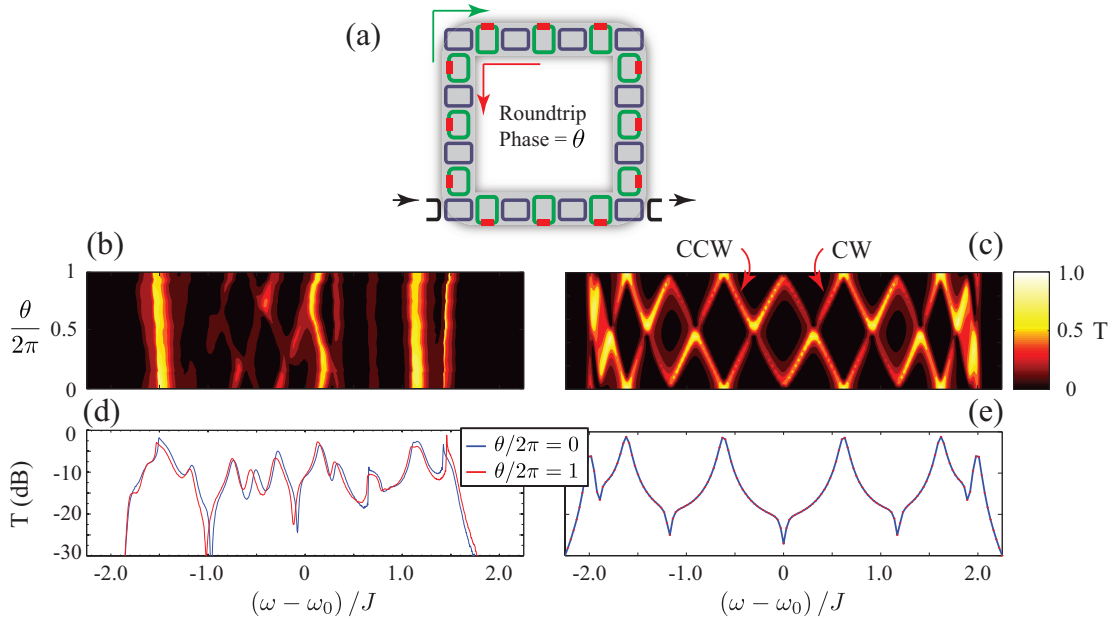


FIG. 4: (a) A ring geometry to investigate gauge coupling to topologically trivial states. The ring supports CW and CCW circulating modes. External flux can be coupled to these states using heaters. (b) Measured and (c) simulated transmission as a function of external flux  $\theta$  and frequency  $\omega$ . The CW and CCW modes move in opposite directions but for a unit increase in flux, they do not change position. (d) Measured and (e) simulated transmission spectra at  $\theta = 0, 2\pi$  overlap well.

by heating the link resonators. Fig. 4b,c show the experimentally observed and the simulated transmission spectra as a function of flux  $\theta$ . The flux lifts the degeneracy of the CW and CCW states and with an increase in the flux, these states move in opposite directions. However, for  $\theta = 2\pi$ , each state returns to its location at  $\theta = 0$ , with measured  $k = 0.03(8)$ . Thus, the absence of spectral flow proves that there is no gauge anomaly in this system. As shown in Fig. 4d, we observe the transmission spectra at  $\theta/2\pi = 0, 1$  exhibit an excellent overlap. However, compared to the simulation, we realize that not all the states can be resolved in the experimental data. Such discrepancy is due to the absence of topological protection of non-chiral states against disorder which leads to coupling between CW and CCW modes.

The remarkable feature of using the gauge anomaly to probe topological invariants is the natural extension of this approach to strongly correlated regimes. Our approach could be applied to photonic systems with strong photon-photon interaction, such as circuit-QED [29] and polariton [30] systems, and also ultracold atoms with topological features [10–13]. The presence of strong interactions could lead to the emergence of various fractional quantum states in the steady-state regime [31]. In particular, the  $1/2$ -Laughlin state corresponds to  $k = 2$  which should be manifested as spectral flow by a unit charge for a  $\theta = 2\pi k$  flux insertion. Therefore, TQFT formalism and corresponding edge anomalies could be a natural approach to probe topological orders and fractional statistics for systems with controllable gauge fields.

[1] X.-G. Wen, *Quantum Field Theory of Many-Body Systems* (Oxford University Press, 2004).

[2] B. Bernevig, T. Hughes, *Topological Insulators and Topological Superconductors* (Princeton University Press, 2013).

[3] D. Hsieh, et al., *Science* **323**, 919 (2009).

- [4] Y. L. Chen, et al., *Science* **325**, 178 (2009).
- [5] M. Konig, et al., *Science* **318**, 766 (2007).
- [6] X.-L. Qi, S.-C. Zhang, *Rev. Mod. Phys.* **83**, 1057 (2011).
- [7] E. Witten, *Communications in Mathematical Physics* **121**, 351 (1989).
- [8] X. G. Wen, *Phys. Rev. B* **41**, 12838 (1990).
- [9] J. Frohlich, T. Kerler, *Nuclear Physics B* **354**, 369 (1991).
- [10] H. Miyake, et al., *Phys. Rev. Lett.* **111**, 185302 (2013).
- [11] G. Jotzu, et al., *Nature* **515**, 237 (2014).
- [12] I. B. Spielman, *Annalen der Physik* **525**, 797 (2013).
- [13] M. Aidelsburger, et al., *Nature. Phys.* **11**, 162 (2015).
- [14] M. Hafezi, J. M. Taylor, *Physics Today* **67**, 68 (2014).
- [15] L. Lu, et al., *Nature Photonics* **8**, 821 (2014).
- [16] Z. Wang, et al., *Nature* **461**, 772 (2009).
- [17] S. Mittal, et al., *Phys. Rev. Lett.* **113**, 087403 (2014).
- [18] M. Hafezi, et al., *Nat. Photonics* **7**, 1001 (2013).
- [19] M. C. Rechtsman, et al., *Nature* **496**, 196 (2013).
- [20] Y. Kraus, et al., *Phys. Rev. Lett.* **109**, 106402 (2012).
- [21] W. Hu, et al., *Phys. Rev. X* **5**, 011012 (2015).
- [22] J. M. Zeuner, et al., *arXiv* **1408.2191** (2014).
- [23] T. Ozawa, I. Carusotto, *Phys. Rev. Lett.* **112**, 133902 (2014).
- [24] M. Hafezi, *Phys. Rev. Lett.* **112**, 210405 (2014).
- [25] C.-E. Bardyn, et al., *New J. Phys.* **16**, 123013 (2014).
- [26] I. P. Levkivskyi, A. Boyarsky, J. Fröhlich, E. V. Sukhorukov, *Phys. Rev. B* **80**, 045319 (2009).
- [27] S. Ganeshan, *PhD Thesis: Quantum Effects in Condensed Matter Systems in Three, Two and One Dimensions* (2012).
- [28] Y. Hatsugai, *Phys. Rev. Lett.* **71**, 3697 (1993).
- [29] A. A. Houck, et al., *Nat. Phys.* **8**, 292 (2012).
- [30] I. Carusotto, C. Ciuti, *Rev. Mod. Phys.* **85**, 299 (2013).
- [31] E. Kapit, et al., *Phys. Rev. X* **4**, 031039 (2014).

**Acknowledgments:** This research was supported by AFOSR, ARO-MURI, Bethe postdoctoral fellowship, NSF Career, LPS-PMO-CMTC and the Physics Frontier Center at the Joint Quantum Institute (JQI-NSF-PFC). We thank M. Levin, A. G. Abanov, A. Lobos, A. Migdall, J. Taylor for fruitful discussions and E. Barnes, M. Davanco, E. Goldschmidt for useful comments on the manuscript.

# Supplementary Information for Observation of the Chern-Simons gauge anomaly

Sunil Mittal<sup>1,2</sup>, Sriram Ganeshan<sup>1,3</sup>, Jingyun Fan<sup>1</sup>, Abolhassan Vaezi<sup>4</sup>,  
 Mohammad Hafezi<sup>1,2,†</sup>

<sup>1</sup>Joint Quantum Institute, NIST/University of Maryland, College Park MD 20742, USA

<sup>2</sup>Department of Electrical Engineering and Institute for Research in Electronics and Applied Physics, University of Maryland, College Park MD 20742, USA

<sup>3</sup>Condensed Matter Theory Center, University of Maryland, College Park MD 20742, USA

<sup>4</sup>Laboratory of Atomic and Solid State Physics, Cornell University, Ithaca NY 14853, USA

†hafezi@umd.edu

## I. SPECTRAL FLOW OF EDGE HAMILTONIAN COUPLED TO A GAUGE FIELD

In this section we will compute the energy spectrum of anomalous edge modes as a function of the net flux  $\theta$ . We start from the action of a single chiral edge coupled to a gauge field.

$$S = \frac{1}{4\pi} \int dx dt \mathcal{L} \quad (S1)$$

$$\mathcal{L} = k D_t \phi D_x \phi - vk(D_x \phi)^2 - \epsilon^{\mu\nu} \eta_\mu \partial_\nu \phi \quad (S2)$$

$$D_\mu \phi = \partial_\mu \phi - \frac{1}{k} \eta_\mu \quad (S3)$$

Note that the edge Lagrangian density  $\mathcal{L}$  is not gauge invariant. This gauge anomaly connects the edge theory to the bulk topological phase through the integer  $k$ .  $k = 1$  corresponds to the integer topological invariant for a non-interacting integer quantum Hall state.  $k = 2$  corresponds to the strongly correlated 1/2-Laughlin state. Gauging this chiral edge results in the anomalous spectral flow which we have experimentally observed in this work. In the following, we will compute the edge spectral flow as a function of the inserted flux.

To this end, we consider the following vertex operators:  $\hat{O}_n(x) \equiv e^{in\phi(x)}$  which creates charge excitations. The first thing we need to do is to measure the charge carried by these operators through computing their commutation relations [4] with the total particle number,  $\hat{Q} = \frac{1}{2\pi} \int_0^L dx \partial_x \phi$ , as follows,

$$[\hat{Q}, \hat{O}_n(y)] = \frac{1}{2\pi} \int dx [\partial_x \phi(x), e^{in\phi(y)}] = \frac{in}{2\pi} \int dx [\partial_x \phi(x), \phi(y)] e^{in\phi(y)} \quad (S4)$$

$$= \frac{in}{2\pi} \int dx \frac{-2\pi i}{k} \delta(x-y) e^{in\phi(y)} = \frac{n}{k} \hat{O}_n(y), \quad (S5)$$

The above relation suggests that  $\hat{O}_n$  operator creates an excitations with  $q = \frac{n}{k}$  fractional charge at  $y$ . In other words, if we apply the operator  $\hat{O}_n$  on an arbitrary state  $|\psi\rangle$ , we get:

$$\langle \psi | \hat{O}_n^\dagger \hat{Q} \hat{O}_n | \psi \rangle = \langle \psi | O_n | \psi \rangle + \frac{n}{k}, \quad (S6)$$

which means that the charge of the arbitrary state increase by  $\frac{n}{k}$ . Using the so-called chiral algebra [1], it can shown that  $n$  must be an integer. Furthermore,  $O_n$  and  $O_{n+k}$  operators are topologically indistinguishable.

We now compute the energy associated with  $O_n$  charge operators. The edge Hamiltonian is defined as,

$$H = \pi \partial_t \phi - \mathcal{L}, \quad \pi = \frac{\delta \mathcal{L}}{\delta(\partial_t \phi)} \quad (S7)$$

In the experiment, we change the gauge only along the edge, therefore, we fix the gauges as  $\eta_t = 0$  and

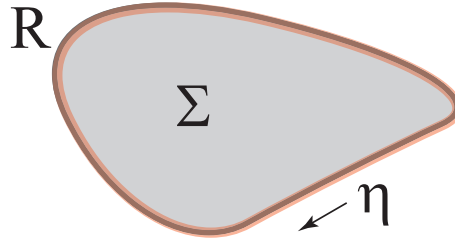


FIG. S1: The bulk region  $\Sigma$  with bulk gauge field  $A_\mu$ . Boundary  $R$  with a gauge field  $\eta(\mu)$  coupled only to the boundary.

$\int_0^L \eta_x(y) dy = \theta$ . For this gauge choice the Hamiltonian reduces to

$$H = \frac{vk}{4\pi} \int dx (\partial_x \phi - \frac{1}{k} \eta_x)^2 = \frac{vk}{4\pi} \int dx (\partial_x \varphi)^2, \quad (\text{S8})$$

where in the last step, for simplicity, we have defined a new field  $\varphi = \phi - \frac{1}{k} \int_0^x \eta_x(y) dy$ . The corresponding bosonic fields satisfy following equal time canonical commutation relations,

$$[\varphi(x), \partial_y \varphi(y)] = \frac{2\pi i}{k} \delta(x - y). \quad (\text{S9})$$

To obtain the spectrum associated with the charge excitations, as defined above, we start evaluating the following commutation relation:

$$\begin{aligned} [H, e^{in\varphi(y)}] &= \frac{vk}{4\pi} \int dx [(\partial_x \varphi(x))^2, e^{in\varphi(y)}] = \frac{vk}{4\pi} \int dx 2in\partial_x \varphi(x) [\partial_x \varphi(x), \varphi(y)] e^{in\varphi(y)} \\ &= vn\partial_y \varphi(x) e^{in\varphi(y)} = -iv\partial_y e^{in\varphi(y)}. \end{aligned} \quad (\text{S10})$$

Since  $\varphi(y) = \phi(y) - \frac{1}{k} \int_0^y \eta_x(x) dx$ , thus:

$$[H, O_n(y)] = v \left( -i\partial_y - \frac{n}{k} \eta_x(y) \right) O_n(y). \quad (\text{S11})$$

By defining the Fourier transform as  $O_n(p) \equiv \int dy e^{-ipy} O_n(y)$ , we obtain the energy spectrum:

$$[H, O_n(p)] = v \left( p - \frac{n}{k} \eta_x \right) O_n(p). \quad (\text{S12})$$

The above equation describes the spectral flow due to flux insertion. It can be understood more intuitively by considering the facts that (i)  $O_n$  operator carries  $q = \frac{n}{k}$  charge. (ii) Energy of fractional quasiparticles has linear dependence on momentum at the edge. (iii) In the presence of  $\eta_x = \frac{\theta}{L}$  gauge field, the momentum operator,  $\hat{p}_x$  must be replaced by the covariant momentum operator,  $\hat{p}_x - q\eta_x$ . These simple observations lead to the spectral flow stating that the energy spectrum of charged excitations varies linearly with the additional coupled flux.

Alternatively, we can evaluate the energy spectrum of the bosonic field  $\phi$ . We diagonalize  $H$  in terms of

creation operators  $a$  which satisfy the following equation

$$[a, H] = \epsilon a, \quad (\text{S13})$$

where  $\epsilon$  is the energy. The most general expression for the operator  $a$  can be written as,

$$a = \int_0^L dy f(y) \partial_y \varphi(y) \quad (\text{S14})$$

Substituting the form of  $a$  into Eq. (S13) we get,

$$-iv \int_0^L dy f'(y) \partial_y \varphi(y) = \epsilon \int_0^L dy f(y) \partial_y \varphi(y). \quad (\text{S15})$$

From the above equation we can write out the following first order differential equation by comparing the coefficient of the operator  $\partial_y \phi$ ,

$$-iv f'(y) = \epsilon f(y) \quad (\text{S16})$$

Solving the above first order differential equation we get,

$$f(y) = A_0 e^{ipy} \text{ with } \epsilon = vp \quad (\text{S17})$$

To obtain the quantization condition due to the closed edge geometry, we identify  $x = 0$  to  $x = L$ . This boundary condition imposes the momentum quantization condition.

$$f(0) = f(L), \quad e^{ipL} = 1, \quad p = \frac{2m\pi}{L} \quad (\text{S18})$$

The edge mode is given by substituting the solution of  $f(y)$  Eq. (S14).

$$a_p = A_0 \int_0^L dy e^{ipy} \partial_y \varphi(y) \quad (\text{S19})$$

The overall normalization constant  $A_0 = \sqrt{\frac{k}{2\pi L|p|}}$  can be fixed to yield the canonical commutation of the oscillator modes  $[a_p, a_{p'}] = \delta(p + p')$ .

$$a_p = \sqrt{\frac{k}{2\pi L|p|}} \int_0^L dy e^{ipy} \partial_y \varphi(y) \quad (\text{S20})$$

In addition to non-zero modes we can also evaluate the zero mode of the energy spectrum for  $a_{p=0}$ . For a closed geometry there is a single zero mode that corresponds to the overall charge on the edge. Note that

this is the point where we note the presence of the net flux threaded.

$$a_0 = \int_0^L dy \partial_y \varphi(y) = \varphi(L) - \varphi(0) = 2\pi\hat{Q} - \frac{1}{k} \int_0^L \eta_x dx \quad (\text{S21})$$

$$a_0 = 2\pi\hat{Q} - \frac{1}{k}\theta \quad (\text{S22})$$

Where  $\hat{Q}$  is the total charge operator. Thus,  $a_0 = \int_0^L dx (D_x \phi) = 2\pi Q - \frac{\theta}{k}$ , where  $Q = \frac{1}{2\pi} \int_0^L dx (\partial_x \phi)$ , and  $\theta = \eta_x L$  are the total particle number at the edge and the net coupled flux, respectively, is a constant of motion and commutes with the edge Hamiltonian. Since,  $[a_0, H] = 0$ , therefore:

$$\frac{d}{dt} \left( \hat{Q}(t) - \frac{1}{2\pi k} \theta(t) \right) = 0. \quad (\text{S23})$$

Consequently,  $Q(t_2) - Q(t_1) = \frac{1}{2\pi k} (\theta(t_2) - \theta(t_1))$ . Accordingly, if the net coupled flux,  $\theta$ , changes by  $2\pi k$  from  $t = t_i$  to  $t = t_f$ , the total number of particles at the edge reduces by one during that time interval. Hence, if we change the net coupled flux by  $2\pi k$ , the number of particles at the edge reduces by one. This missing particle is a consequence of the gauge invariance of bulk+edge, where a particle is transferred from the edge to the bulk. This change in particle number can be understand more intuitively from spectral flow described below.

## II. EIGENVALUES OF SQUARE ANNULUS AS FUNCTION OF EXTERNAL FLUX

Fig. S2 shows the eigenvalues of this system as a function of the external phase  $\theta$ , the total phase introduced by a loop of heaters. We observe that with an increase in the external flux, all the edge states shift outwards or inwards. The CW-propagating outer edge states in the first bandgap move toward lower energies, whereas the CCW-propagating outer edge states in the third bandgap move toward higher energies. The inner edge states move exactly opposite to the outer edge states. More importantly, for a  $2\pi$  increase in magnetic flux, each set of states shift exactly by one, their winding number. The direction of shift is indicated by the sign of the winding number. After a  $2\pi$  increase in the flux, the spectrum returns back to its original shape with  $\theta = 0$ .

## III. COUPLING EXTERNAL GAUGE FIELD

The implementation of a uniform synthetic magnetic field for photons and coupling an external gauge field to the edge states hinges on the use of link resonators to couple the site resonators. By vertically displacing the link resonator we can introduce a direction dependent, fixed, hopping phase for the photons hopping between site resonators [2, 3]. The fabrication of heaters above the link resonator waveguides enables us to tune this hopping phase. Here, we analyze a system of two site resonators coupled by a link resonator, with a heater on the link resonator waveguide. The heater introduces a phase  $2\theta$ . We show this system is equivalent to two site rings coupled by an effective coupling rate  $J$  and a hopping phase  $\theta_T$ , where  $\theta_T$  includes the fixed phase incurred due vertical shift of the link resonator and the tunable external gauge flux introduced by the heater.

We first analyze the system of site rings coupled by a link ring, using the rigorous transfer matrix method. The site resonators have a length  $L$  and the link ring  $L + \eta$ . Furthermore, the link ring is vertically displaced

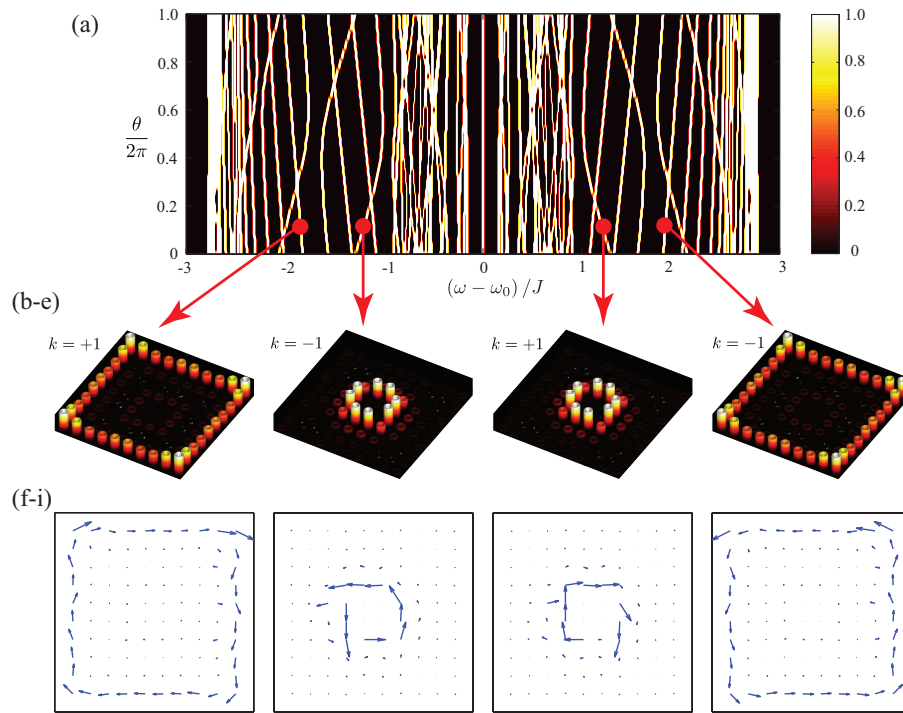


FIG. S2: (a) Shifting of eigenvalues as a function of external magnetic flux  $\theta$ . The annulus now supports two sets of edge states, at the outer (b,e) and the inner edges (c,d). In a given bandgap, the outer (f,i) and the inner (g,h) edge states circulate around the lattice in opposite directions because of their opposite group velocity. Furthermore, in the energy spectrum (a), the clockwise and the counterclockwise circulating states move in opposite directions because of their winding number which is  $\pm 1$ .

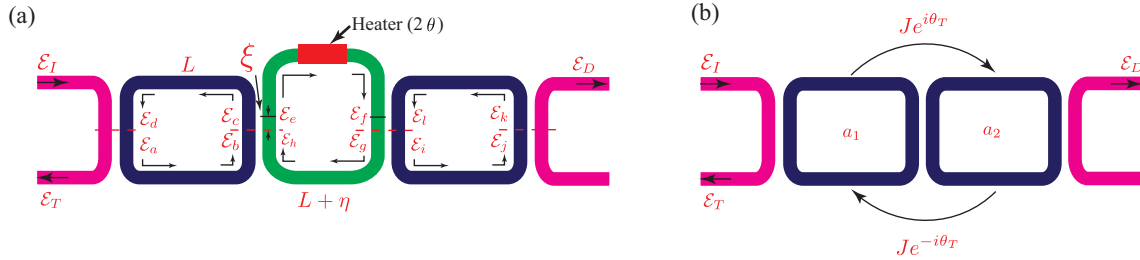


FIG. S3: (a) A system of two site resonators, coupled by a link resonator with a heater, and also coupled to input and output waveguides. The figure labels the fields for the transfer matrix analysis. (b) Effective description of the system in coupled mode theory. The effect of the link resonator is contained in the coupling rate  $J$  and hopping phase  $\theta_T$  which accounts for the vertical shift of the link ring and the phase introduced by the heater.

by length  $\xi$  and has a heater on the upper arm which introduces a phase  $2\theta$ . We label the fields as shown in

Fig. S3. Using transfer matrix formalism, we can relate the different field amplitudes as [3]

$$\begin{pmatrix} \mathcal{E}_d \\ \mathcal{E}_a \end{pmatrix} = \frac{1}{i\kappa_i} \begin{pmatrix} -t_i & 1 \\ -1 & t_i \end{pmatrix} \begin{pmatrix} \mathcal{E}_I \\ \mathcal{E}_T \end{pmatrix}, \quad (\text{S24})$$

$$\begin{pmatrix} \mathcal{E}_c \\ \mathcal{E}_b \end{pmatrix} = \begin{pmatrix} e^{-(i\beta-\alpha)\frac{L}{2}} & 0 \\ 0 & e^{(i\beta-\alpha)\frac{L}{2}} \end{pmatrix} \begin{pmatrix} \mathcal{E}_d \\ \mathcal{E}_a \end{pmatrix}, \quad (\text{S25})$$

$$\begin{pmatrix} \mathcal{E}_e \\ \mathcal{E}_h \end{pmatrix} = \frac{1}{i\kappa} \begin{pmatrix} -t & 1 \\ -1 & t \end{pmatrix} \begin{pmatrix} \mathcal{E}_c \\ \mathcal{E}_b \end{pmatrix}, \quad (\text{S26})$$

$$\begin{pmatrix} \mathcal{E}_f \\ \mathcal{E}_g \end{pmatrix} = \begin{pmatrix} e^{(i\beta-\alpha)(\frac{L+\eta}{2}+2\xi)} e^{i2\theta} & 0 \\ 0 & e^{-(i\beta-\alpha)(\frac{L+\eta}{2}-2\xi)} \end{pmatrix} \begin{pmatrix} \mathcal{E}_e \\ \mathcal{E}_h \end{pmatrix}, \quad (\text{S27})$$

$$\begin{pmatrix} \mathcal{E}_l \\ \mathcal{E}_i \end{pmatrix} = \frac{1}{i\kappa} \begin{pmatrix} -t & 1 \\ -1 & t \end{pmatrix} \begin{pmatrix} \mathcal{E}_f \\ \mathcal{E}_g \end{pmatrix}, \quad (\text{S28})$$

$$\begin{pmatrix} \mathcal{E}_k \\ \mathcal{E}_j \end{pmatrix} = \begin{pmatrix} e^{-(i\beta-\alpha)\frac{L}{2}} & 0 \\ 0 & e^{(i\beta-\alpha)\frac{L}{2}} \end{pmatrix} \begin{pmatrix} \mathcal{E}_l \\ \mathcal{E}_i \end{pmatrix}, \quad (\text{S29})$$

$$\begin{pmatrix} \mathcal{E}_D \\ 0 \end{pmatrix} = \frac{1}{i\kappa_i} \begin{pmatrix} -t_i & 1 \\ -1 & t_i \end{pmatrix} \begin{pmatrix} \mathcal{E}_k \\ \mathcal{E}_j \end{pmatrix} \quad (\text{S30})$$

Here,  $t_i$  and  $k_i$  are the field transmission and cross coupling coefficients for coupling of link rings to the input and output ports, and  $t, k$  are those for the coupling between the rings.  $\beta$  and  $\alpha$  are the propagation constant and the loss coefficient in the ring resonator waveguide, respectively. These equations then give the field at the drop port as

$$\mathcal{E}_D = \frac{e^{i\theta} e^{i2\beta\xi} \kappa^2 \kappa_i^2 \mathcal{E}_I}{e^{-(i\beta+\alpha)L} e^{-\frac{i\beta\eta+i2\theta}{2}} \left( e^{i2\theta} e^{i\beta(L+\eta)} (t_i - t) (e^{\alpha L} t - e^{i\beta L} t_i) + (1 - t t_i) (e^{2\alpha L} - e^{(i\beta+\alpha)L} t t_i) \right)}. \quad (\text{S31})$$

Here we have assumed that the extra length  $\eta$  of the link ring and its vertical shift  $\xi$  are negligible compared to  $L$ , so that the loss incurred in these extra lengths is insignificant. In our experimental system,  $\eta = 320$  nm,  $\xi = 80$  nm and  $L \approx 70\mu\text{m}$ , which justifies the above assumption.

In the weak coupling limit, i.e., when  $\kappa_i, \kappa \ll 1$  and  $t_i, t \approx 1$ , the expression for the drop field can be simplified to

$$\mathcal{E}_D = \frac{e^{i\theta} e^{i2\beta\xi} \kappa^2 \kappa_i^2 \mathcal{E}_I}{2k^2 \left( \frac{\kappa_i^2}{2} + \alpha L + i\beta L \right) \cos \left( \frac{\beta\eta+2\theta}{2} \right) - 2i \left( \frac{\kappa^4}{4} + \left( \frac{\kappa_i^2}{2} + \alpha L + i\beta L \right)^2 \right) \sin \left( \frac{\beta\eta+2\theta}{2} \right)}. \quad (\text{S32})$$

This system of two site rings coupled by a link ring can be equivalently described by a system involving only the site rings, coupled by coupling rate  $J$  and a hopping phase  $\pm\theta_T$  (Fig. S3b). Specifically, we use single mode approximation for the site rings and employ the coupled mode theory to capture the effect of the link ring in  $J$  and  $\theta_T$ . In the coupled mode theory, the rate equations for the time evolution of the site

ring energy amplitudes,  $a_1(t)$  and  $a_2(t)$ , are

$$\frac{da_1}{dt} = (-i\omega_0 - \kappa_{ex} - \kappa_{in}) a_1 - iJ e^{-i\theta_T} a_2 - \sqrt{2\kappa_{ex}} \mathcal{E}_I \quad (\text{S33})$$

$$\frac{da_2}{dt} = (-i\omega_0 - \kappa_{ex} - \kappa_{in}) a_2 - iJ e^{i\theta_T} a_1, \quad (\text{S34})$$

where  $\kappa_{ex}$  is the coupling of the site rings to the input and output waveguides and  $\kappa_{in}$  is the resonator loss rate. A steady-state solution of the above equations for a plane wave excitation of frequency  $\omega$  gives

$$a_1 = \frac{(i(\omega - \omega_0) - \kappa_{ex} - \kappa_{in}) \sqrt{2\kappa_{ex}} \mathcal{E}_I}{(i(\omega - \omega_0) - \kappa_{ex} - \kappa_{in})^2 + J^2} \quad (\text{S35})$$

$$a_2 = \frac{iJ e^{i\theta_T} a_1}{(i(\omega - \omega_0) - \kappa_{ex} - \kappa_{in})}. \quad (\text{S36})$$

Then, the field output at the drop port  $\mathcal{E}_D^{\text{CMT}} = \sqrt{2\kappa_{ex}} a_2$  is

$$\mathcal{E}_D^{\text{CMT}} = \frac{2i e^{i\theta_T} J \kappa_{ex} \mathcal{E}_I}{(i(\omega - \omega_0) - \kappa_{ex} - \kappa_{in})^2 + J^2}. \quad (\text{S37})$$

To compare this expression for the drop field to that derived using the transfer matrix approach, we use the relations [3]

$$\beta = \frac{(\omega_0 - \omega)}{v_g} \quad (\text{S38})$$

$$\kappa_{in} = \alpha v_g \quad (\text{S39})$$

$$\kappa_{ex} = \frac{\kappa_i^2 v_g}{2L} \quad (\text{S40})$$

$$J = \frac{\kappa^2 v_g}{2L}. \quad (\text{S41})$$

The drop field in the transfer matrix formulation is then

$$\mathcal{E}_D = \frac{2e^{i\theta_T} J \kappa_{ex} \mathcal{E}_I}{2J(i(\omega_0 - \omega) + \kappa_{ex} + \kappa_{in}) \cos\left(\frac{\beta\eta + 2\theta}{2}\right) + i\left(J^2 + (i(\omega_0 - \omega) + \kappa_{ex} + \kappa_{in})^2\right) \sin\left(\frac{\beta\eta + 2\theta}{2}\right)}, \quad (\text{S42})$$

where  $\theta_T = 2\beta\xi + \theta$ . We see that the introduction of a phase  $2\theta$  in one of the arms of the link resonator results in an additional hopping phase of  $\theta$ . Further, for  $\beta\eta + 2\theta = (\pi, 3\pi, 5\pi, \dots)$ , i.e., when the link ring is anti-resonant to the site rings, the two expressions are identical. Because the link ring is anti-resonant, it does not store any energy and simply acts as a waveguide, without affecting the coupling between the site rings.

When  $\beta\eta + 2\theta$  is not an odd-integer multiple of  $\pi$ , the two expressions for the drop field, derived using the coupled mode theory and the transfer matrix method, are identical if we use an effective coupling rate  $J^{\text{eff}} = J / \sin\left(\frac{\beta\eta + 2\theta}{2}\right)$  and shift the resonance frequency of the site rings as  $\omega_0^{\text{eff}} = \omega_0 + J \cot\left(\frac{\beta\eta + 2\theta}{2}\right)$ . In our experiment, we design the link rings such that  $\beta\eta = \pi$ . Further, we distribute the external gauge flux  $\theta$  over 12 heaters so that the introduction of external gauge flux  $\theta$  results in negligible correction to coupling rate  $J$  and a small shift in the resonance frequency of the site rings. For example, for  $\theta = 2\pi$  divided over

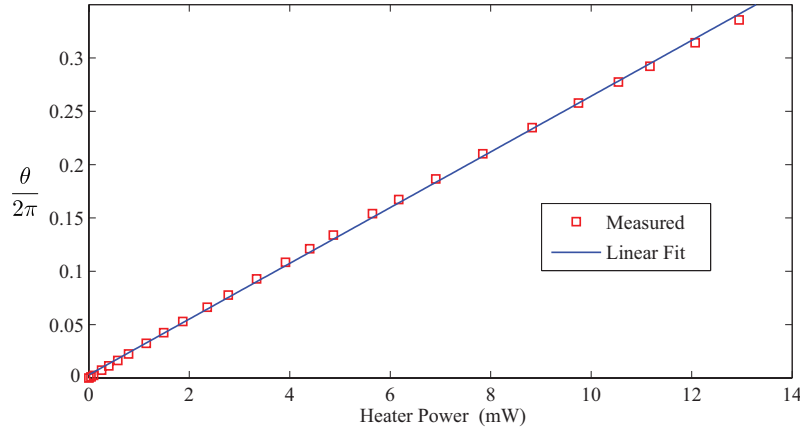


FIG. S4: Measured phase shift in an ADF, as a function of the heater power. The acquired phase shift (in units of  $2\pi$ ) increases linearly with the heater power (in mW), with a slope of 0.026(1).

12 link rings, the correction to the coupling rate  $J$  is only 3.5%. However, the shift in resonance frequency  $\Delta\omega_0$  is  $0.27J$ , which adds to disorder in the lattice.

Our system supports two degenerate spin states - circulating CW and CCW in the ring resonators. The above discussion is for CCW state. Following similar procedure for CW state (spin flipped) results in a negative sign for the gauge flux theta.

#### IV. HEATER CALIBRATION

We used an add-drop filter (ADF - a ring coupled to two waveguides) with a heater, to calibrate the phase shift acquired for a unit heater power. The ADF ring has exactly the same dimensions as the rings in the 2D array. The ring waveguides are designed to be 510 nm wide to ensure single mode (TE) operation at telecom wavelengths and the typical ring perimeter is  $\approx 70\mu\text{m}$ . The coupling gap between the ring waveguides is 140 nm which gives a coupling rate  $J = 40.6$  GHz. The heater introduces a phase shift  $\theta$  in the ADF ring waveguide and shifts its resonance frequency by  $\Delta\omega_0$ , such that

$$\theta = \frac{\Delta\omega_0}{FSR} 2\pi, \quad (\text{S43})$$

where  $FSR = 2\pi \frac{v_g}{L}$  is the free spectral range of the ring,  $v_g$  is the group velocity and  $L$  is the length of the ring. Measuring the resonance frequency shift as a function of heater power gives us an estimate of the phase difference introduced by the heater. We used an ADF ring which had exactly the same dimensions as the rings in the square annulus and the chain of resonators. Fig. S4 shows the observed phase shift as a function of heater power. The heater resistance was  $\approx 120$  Ohms and the voltage applied to the heater ranged from 0-3 Volts. We see that the acquired phase increases linearly with the heater power.

For the square annulus and the chain geometry, we used this calibration curve to estimate  $\theta$  for a given voltage applied to the heaters. For the annulus, all the 12 heaters in the outer (and the inner) loop (Fig. 1c) were serially connected. The measured resistance was 1.4 KOhms and the applied heater voltage across the loop ranged from  $\approx 8$ -14 Volts, which introduced the phase  $\theta = \pi - 3\pi$ . Similarly, in the chain of rings (Fig. 4a), all the 20 heaters were connected serially, giving a total resistance of 2.31 KOhms. The total voltage applied across the heaters ranged from  $\approx 0 - 13$  Volts, for  $\theta = 0 - 2\pi$ . Furthermore, as we saw in the previous section, the transfer matrix analysis of a system of two site rings, coupled by a link ring, shows

that if the heater introduces an extra phase  $2\theta$  in one of the arms, the effective hopping phase (using CMT) between the link rings is  $\theta$ . We have included this factor of 2 in our calculations.

## V. ESTIMATION OF INTEGER $K$

To estimate the value of index  $k$ , we use the edge state peaks in the transmission spectra at  $\theta = 0$  and  $2\pi$  (see Fig. 2). For each band (CW and CCW), we measure the shift of the edge state resonances as  $\theta$  increases from 0 to  $2\pi$  and the separation between the edge state resonances at  $\theta = 0$ . The integer  $k$  is then the ratio of the shift of the edge states to the separation between the edge states.

## VI. DISORDER ESTIMATION

In our design, the heaters are placed 600 nm above the link resonator waveguides. Because of this, the heat is not confined only to the ring beneath the heater but instead also heats the neighboring site resonators. Using a three ring device where two site rings are coupled by a link ring, we estimate that for every unit shift in resonance frequency of the link ring, the site rings move by 0.3 units. The small curvature observed in the shifting of edge states is also a result of this disorder. We have accounted for this disorder in our simulation. Moreover, because of this disorder we find that for the square annulus, the transmission spectrum retains its shape in the range  $\theta \approx \pi - 3\pi$ . In our measurements reported in Fig. 2, the external gauge flux has been normalized to  $\theta = 0 - 2\pi$ .

Furthermore, because of this nonlocal behavior of the heaters, the device spectrum shifts towards lower frequencies as we increase the voltage applied to the heaters. We have adjusted for this overall shift of the transmission spectra. For each spectrum, we choose two edge state peaks, one each on CW and CCW bands and align all the spectra to the center of these two peaks. The resulting plot thus shows only the differential shift between the two edge state bands. For the ring geometry, the measured spectrum at  $\theta = 2\pi$  in Fig. 4d has been scaled along the frequency axis (by a factor of 0.98), to offset the dispersion effect (due to the overall shift) which results in slight broadening of the spectrum.

---

[1] X.-G. Wen, *Quantum Field Theory of Many-Body Systems* (Oxford University Press, 2004).

[2] M. Hafezi, et al., *Nature Phys.* **7**, 907 (2011).

[3] M. Hafezi, et al., *Nat. Photonics* **7**, 1001 (2013).

[4] Note that the conjugate variable for  $\phi(x)$  is given by  $\pi = \frac{\delta \mathcal{L}}{\delta(\partial_t \phi)} = k \partial_x \phi$ , therefore, we have the following commutation relationship:  $[\phi(y), \partial_x \phi(x)] = \frac{2\pi i}{k} \delta(x - y)$ .